

A spiral galaxy’s mass distribution uncovered through lensing and dynamics

W. Trick^{1*}, G. van de Ven¹ and A. Dutton¹

¹*Max-Planck-Institute for Astronomy, Königstuhl 17, 69117 Heidelberg, Germany*

Accepted ?????. Received ????; in original form ????.

ABSTRACT

We analyse the stellar and dark matter distribution in the spiral galaxy SDSS J1331+3638 (J1331) by means of two independent methods: gravitational lensing and dynamical Jeans modelling. Hubble Space Telescope (HST) imaging by Treu et al. (2011) reveals, that J1331’s bulge is superimposed by a quadruplet of extended lensing images. By fitting a gravitational potential model to the image positions, we constrain the mass inside the Einstein radius ($R_{\text{ein}} = 0.91 \pm 0.02$ arcsec) to within 4% ($M_{\text{ein}} = (7.8 \pm 0.3) \cdot 10^{10} M_{\odot}$). From Multi-Gaussian Expansions (MGE) of J1331’s surface brightness distribution we find that J1331 has an apparent I-band magnitude of $m_I \simeq 15.8$ mag, a total luminosity of $L_{I,\text{tot}} \simeq 5.6 \cdot 10^{10} L_{I,\odot}$ and an effective radius of $R_{\text{eff}} \simeq 2.6$ arcsec = 5.6 kpc.

According to the long-slit major axis stellar kinematics from Dutton et al. (2013), J1331 has a counter-rotating stellar core inside ~ 2 arcsec. We model the observed stellar kinematics in J1331’s central regions by finding MGE models for the stellar and dark matter distribution that solve the axisymmetric Jeans equations. We find that J1331 requires a steep total mass-to-light ratio gradient in the center to reproduce the observed stellar kinematics. The best fit dynamical model predicts a total mass inside the Einstein radius consistent with the lens model, and vice versa the lens model gives an successful prediction for the observed kinematics in the galaxy center. For a dynamical model including a NFW dark matter halo, we constrain the halo to have virial velocity $v_{200} \simeq 240 \pm 40$ km/s and a concentration of $c_{200} \simeq 8 \pm 2$ in case of a moderate tangential velocity anisotropy of $\beta_z \simeq 0.4 \pm 0.1$. The NFW halo models can successfully reproduce the signatures of J1331’s counter-rotating stellar core and predict J1331’s rotation curve at larger radii. However, all these models were more massive than expected from the gas rotation curve at larger radii, and failed to reproduce the steep drop in measured velocity dispersion at [TO DO: WHAT RADIUS???]. This could indicate a non-trivial re-distribution of matter due a possible minor merger event in J1331’s past.

Key words: blabla – blabla: bla.

* E-mail: trick@mpia.de

1 INTRODUCTION

[TO DO]

Characteristics of J1331: Lensing

- at redshift $z_d \simeq 0.113$ [TO DO: REF]
 - large reddish bulge
 - superimposed by quadruplet of extended bluish images
- at a redshift of $z_s \simeq 0.254$ [TO DO: REF]
- lensed object might be a star-forming blob of a background galaxy.

Data used

- Hubble Space Telescope (HST) imaging by Treu et al. (2011)

[TO DO]

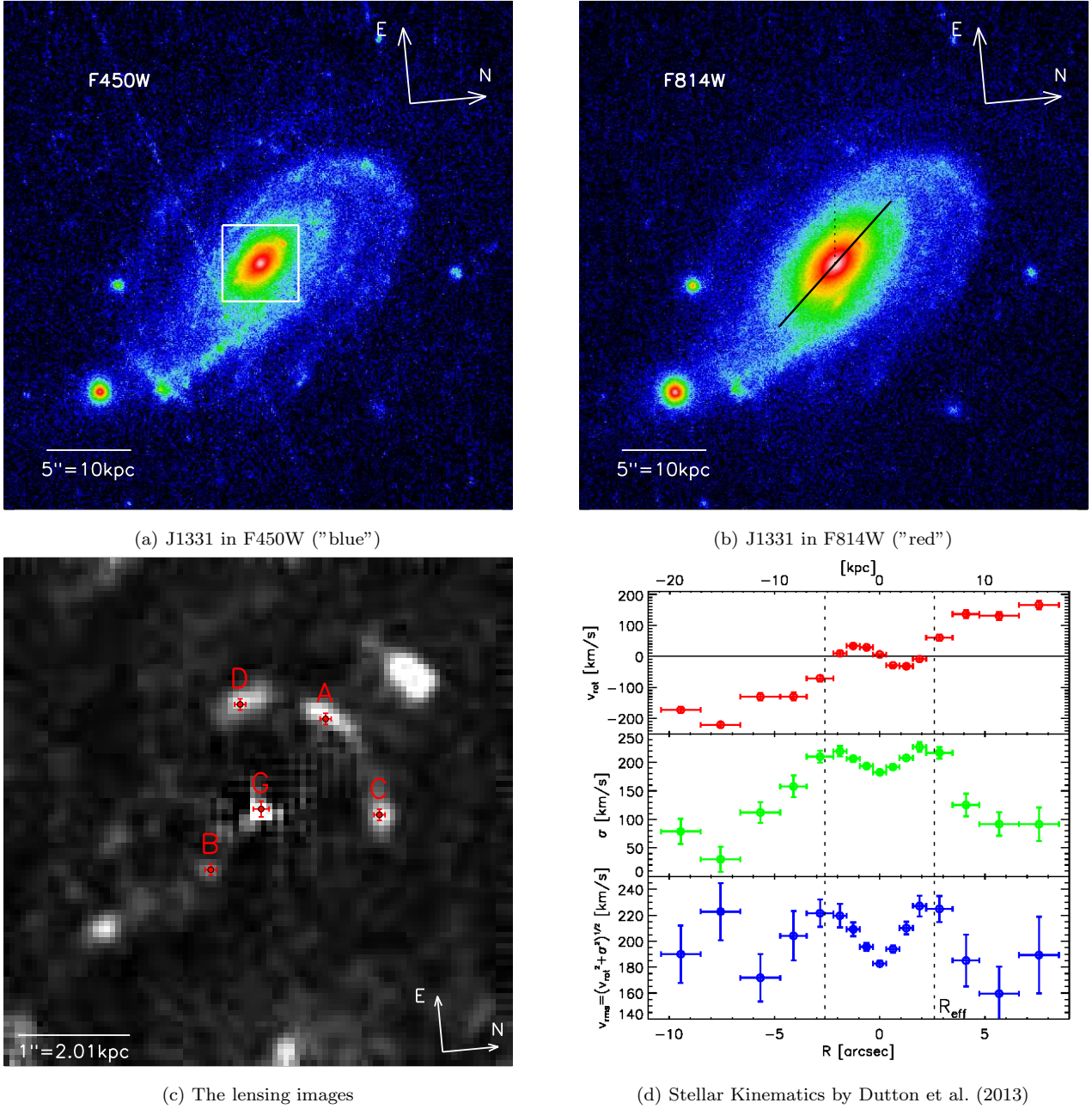


Figure 1. Hubble Space telescope (HST) images and stellar kinematics of the galaxy SDSS J1331+3638 (J1331), which has a large counter-rotating core and whose bulge acts as a strong lens for a bluish background source. *Panel (a) and (b):* HST images of J1331 by Treu et al. (2011) in two filters, F450W in panel (a) and F814W in panel (b). The galaxy's coordinates on the sky are right ascension $\alpha = 202.91800^\circ$ and declination $\delta = 36.46999^\circ$ (epoch J2000). Image orientation and scaling are indicated in panel (a); the scaling transformation from arcseconds to the physical size of the galaxy in kpc uses the galaxy's redshift $z_d = 0.113$ (Brewer et al. 2012). The black solid line in panel (a) shows the orientation of the major-axis. The line has a length of 10 arcsec and indicates the region within which we carry out the Jeans modelling. (NOT ALL THE TIME?????) *Panel (c):* The central region of J1331 in F450W, surface brightness subtracted. An IRAF ellipse fit to the F450W surface brightness in panel (a) was subtracted from the image. The (smoothed) residuals within the white square in panel (a) are shown in panel (c). Four bright blobs (A,B,C and D) become visible, which are arranged in a typical strong lensing configuration around the center of the galaxy (G). *Panel (d):* Stellar Kinematics along the galaxy's major axis as measured by Dutton et al. (2013), line-of-sight rotation velocity v_{rot} , line-of-sight velocity dispersion σ and the rms-velocity $v_{\text{rms}} = \sqrt{v_{\text{rot}}^2 + \sigma^2}$. The dotted line in panel (b) indicates the galaxy's effective half-light radius (in the F814W filter), $R_{\text{eff}} = 2.6'' = 5.2$ kpc. The v_{rot} curve reveals that J1331 is counter-rotating within R_{eff} . TO DO: Add (x,y) axis in figure b).??????

2 DATA

[TO DO]

- Hubble Space telescope (HST) imaging by Treu et al. (2011) in two filters (F450W and F814W)
- I filter: for surface brightness distribution of J1331's bulge for Jeans modelling
- ??? filter: to identify bluish lensing images

3 MODELLING

3.1 Multi-Gaussian Expansion Formalism

[TO DO]

3.2 Strong Gravitational Lensing Formalism and Lens Model

Lensing Formalism. A gravitational lens is a mass distribution, whose gravitational potential Φ acts as a lens for light coming from a source positioned somewhere on a plane behind the lens. The angular diameter distance from the observer to the lens is D_d , to the source plane it is D_s and the distance between the lens and source plane is D_{ds} . The deflection potential of the lens is its potential, projected along the line of sight z and rescaled to

$$\psi(\vec{\theta}) := \frac{D_{ds}}{D_d D_s} \frac{2}{c^2} \int \Phi(\vec{r} = D_d \vec{\theta}, z) dz, \quad (1)$$

where $\vec{\theta}$ is a 2-dimensional vector on the plane of the sky. The light from the source at $\vec{\beta} = (\xi, \eta)$ is deflected according to the lens equation

$$\vec{\beta} = \vec{\theta}_i - \vec{\nabla}_{\theta} \psi(\vec{\theta}) \Big|_{\vec{\theta}_i} \quad (2)$$

into an image $\vec{\theta}_i = (x_i, y_i)$. The gradient of the deflection potential $\vec{\nabla}_{\theta} \psi(\vec{\theta})$ is equal to the angle by which the light is deflected multiplied by D_{ds}/D_s .

The total time delay of an deflected light path through $\vec{\theta}$ with respect to the unperturbed light path is given by

$$\Delta t(\vec{\theta}) = \frac{(1+z_d)}{c} \frac{D_d D_s}{D_{ds}} \left[\frac{1}{2} (\vec{\theta} - \vec{\beta})^2 - \psi(\vec{\theta}) \right], \quad (3)$$

(Narayan & Bartelmann 1999). According to Fermat's principle the image positions will be observed at the extrema of $\Delta t(\vec{\theta})$.

The inverse magnification tensor

$$\mathcal{M}^{-1} \equiv \frac{\partial \vec{\beta}}{\partial \vec{\theta}} \stackrel{(2)}{=} \left(\delta_{ij} - \frac{\partial^2 \psi}{\partial \theta_i \partial \theta_j} \right) \quad (4)$$

describes how the source position changes with image position. It also describes the distortion of the image shape for an extended source and its magnification due to lensing according to

$$\mu \equiv \frac{\text{image area}}{\text{source area}} = \det \mathcal{M}.$$

Lines in the image plane for which the magnification becomes infinite, i.e. $\det \mathcal{M}^{-1} = 0$, are called *critical curves*. The corresponding lines in the source plane are called *caustics*. The position of the source with respect to the caustic determines the number of images and their configuration and shape with respect to each other.

The *Einstein mass* M_{ein} and *Einstein radius* R_{ein} are defined via the relation

$$M_{\text{ein}} \equiv M_{\text{proj}}(< R_{\text{ein}}) \stackrel{!}{=} \pi \Sigma_{\text{crit}} R_{\text{ein}}^2,$$

where $\Sigma_{\text{crit}} \equiv \frac{c^2}{4\pi G} \frac{D_s}{D_d D_{ds}}$ is the critical density and $M_{\text{proj}}(< R_{\text{ein}})$ is the mass projected along the line-of-sight within R_{ein} . M_{ein} is similar to the projected mass within the critical curve M_{crit} .

Lens Model. Following Evans & Witt (2003) we assume a scale-free model

$$\psi(R', \theta) = R'^{\alpha} F(\theta)$$

for the lensing potential, consisting of an angular part $F(\theta)$ and a power-law radial part, with (R', θ) being polar coordinates on the plane of the sky. The case $\alpha = 1$ corresponds to a flat rotation curve. We expand $F(\theta)$ into a Fourier series,

$$F(\theta) = \frac{a_0}{2} + \sum_{k=1}^{\infty} (a_k \cos(k\theta) + b_k \sin(k\theta)). \quad (5)$$

For this scale-free lens model the lens equation (2) becomes

$$\begin{pmatrix} \xi \\ \eta \end{pmatrix} = \begin{pmatrix} R'_i \cos \theta_i - R'_i{}^{\alpha-1} (\alpha \cos \theta_i F(\theta_i) - \sin \theta_i F'(\theta_i)) \\ R'_i \sin \theta_i - R'_i{}^{\alpha-1} (\alpha \sin \theta_i F(\theta_i) + \cos \theta_i F'(\theta_i)) \end{pmatrix} \quad (6)$$

(Evans & Witt 2003), where $F'(\theta) = \partial F(\theta)/\partial \theta$. When we fix the slope α , then the lens equation is a purely linear problem and can be solved numerically for the source position (ξ, η) and the Fourier parameters (a_k, b_k) given one observed image at position $(x_i = R'_i \cos \theta_i, y_i = R'_i \sin \theta_i)$.

	A	B	C	D	G
x_i [pixel]	12.1	-8.5	21.7	-3.3	$0.5 \pm \sqrt{2}$
y_i [pixel]	16.6	-10.4	-0.5	19.2	$0.5 \pm \sqrt{2}$

Table 1. Positions of the lensing images (A-D) and the galaxy center (G) in fig. 1c. The image positions were determined from the lens subtracted image for J1331 in figure 4 of Brewer et al. (2012), rotated to the (x, y) coordinate system in fig. 1c. The pixel scale is 1 pixel = 0.05 arcsec and the error of each image position is ± 1 pixel. *SMALL PROBLEM: Somehow I used $\sqrt{2}$ pixel as the error on the galaxy center in the Monte Carlo sampling code instead of the 0.5 pixel I claim here. Should I change this table and the error bars in the figures to match this bug???*

3.3 Fitting the Lens Model to the Image Positions

Image Positions. We determine the positions of the lensing images by first subtracting a smooth model for the galaxy’s surface brightness from the original image. As models we use MGE fits (cf. §??) and IRAF ellipse fits (???) to the galaxy in each the F450W and F814W filter. (For example the MGE we use for F814W is the MGE given in tab. 3 convolved with the PSF in tab. 2.) The lensing images become then visible in the residuals (see fig. 1c). Because the lensing images are extended, we use the position of the brightest pixel in each of the images. We also use the F814W-MGE subtracted residuals from Brewer et al. (2012). The lensing positions as determined from the latter are given in tab. 1. The scatter of lensing positions as determined from subtracting different surface brightness models from the galaxy in different filters gives an error of ± 1 pixel on the image positions.

Fitting. As described in §?? our lensing model has the following free parameters: the source position (ξ, η) , and the radial slope α and Fourier parameters (a_k, b_k) of the lens mass distribution in eq. (3.2) and (5). We want to find the lensing model which minimizes for all four images the distance between the observed image positions $\vec{\theta}_{oi}$ and those predicted by the lensing model $\vec{\theta}_{pi}$. Because we want to avoid solving the lens equation (cf. eq. (2) and (6)) for θ_{pi} , we follow Kochanek (1991) and cast the calculation back to the source plane using the magnification tensor in eq. (4):

$$\begin{aligned} \chi_{\text{lens}}^2 &= \sum_{i=1}^4 \left| \begin{pmatrix} \frac{1}{\Delta_x} & 0 \\ 0 & \frac{1}{\Delta_y} \end{pmatrix} (\vec{\theta}_{pi} - \vec{\theta}_{oi}) \right|^2 \\ &\simeq \sum_{i=1}^4 \left| \begin{pmatrix} \frac{1}{\Delta_x} & 0 \\ 0 & \frac{1}{\Delta_y} \end{pmatrix} \mathcal{M}|_{\vec{\theta}=\vec{\theta}_{oi}} \begin{pmatrix} \xi - \tilde{\xi}_i \\ \eta - \tilde{\eta}_i \end{pmatrix} \right|^2, \end{aligned}$$

where (Δ_x, Δ_y) are the measurement errors of the image positions $\vec{\theta}_{oi}$. $\mathcal{M}|_{\vec{\theta}=\vec{\theta}_{oi}}$ is the magnification tensor and $(\tilde{\xi}_i, \tilde{\eta}_i)$ the source position according to the lens equation evaluated at $\vec{\theta}_{oi}$. Following van de Ven et al. (2010) we add a term

$$\chi_{\text{shape}}^2 = \lambda \sum_{k \geq 3} \frac{(a_k^2 + b_k^2)}{a_0^2}$$

which forces the shape of the mass distribution to be close to an ellipse. The total χ^2 to minimize is therefore

$$\chi^2 = \chi_{\text{lens}}^2 + \chi_{\text{shape}}^2$$

We set $a_1 = b_1 = 0$, which corresponds to the choice of origin; in this case the center of the galaxy.

To be able to constrain the slope α , we would have needed flux ratios for the images as in van de Ven et al. (2010). But the extended quality of the images and the uncertainty in surface brightness subtraction makes flux determination too unreliable and we do not include them in the fitting. Even though the constraint from just the image position fit on α is very weak, we were however able to show that the image positions in tab. 1 minimize χ^2 at $\alpha = 1$ and also our other image position sets from different models and filters are consistent with a flat rotation curve. In the following we therefore set $\alpha = 1$.

3.4 Jeans Axisymmetric Modelling (JAM)

[TO DO]

4 RESULTS

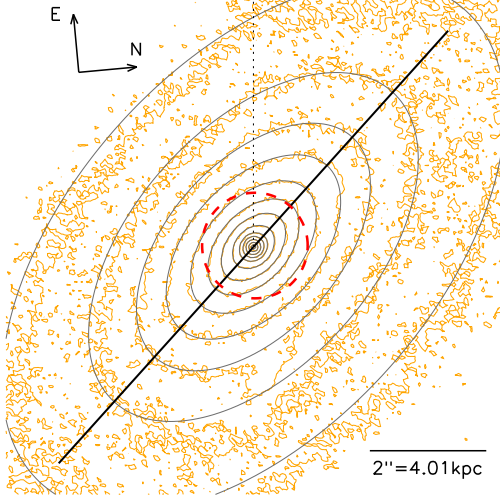


Figure 2. ??? MGE as used in the dynamical modelling ??? [TO DO: nice caption]

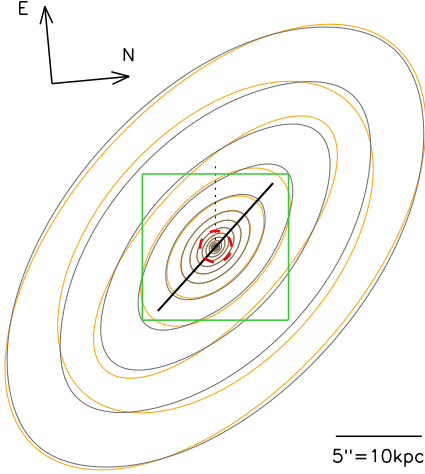


Figure 3. ??? [TO DO: caption]

Table 4. Galaxy Parameters of J1331

redshift	z_d	0.113	(Brew
angular diameter distance	D_d [Mpc]	414	
scaling	1 kpc / 1 arcsec	2.006	
position angle	ϕ [degrees]	wrt what???	
average axis ratio	q'	0.598	
average ellipticity	$\epsilon = 1 - q'$	0.402	
apparent F814W magnitude	m_{F814W} [mag]	15.77	
total F814W luminosity	$L_{tot,F814W}$ [$10^{10} L_\odot$]	5.6	
effective half-light radius	R_{eff} [arcsec]	2.6	
	R_{eff} [pc]	5.2	

4.1 Surface Photometry for J1331 with MGE

[TO DO]

[TO DO: Stuff to mention]

- fit sof MGE to J1331s surface brightness within ~ 2 half-light radii, and to an Iraf Ellipse model for J1331's outer regions, make it possible to easily deconvolve the hst images with its PSF.
- the deporjecten if the galaxy under the assumption of oblate axusymmetry and an estimated inclination of $\sim 70^\circ$ can be performed analytically.

Table 2. PSF F814W MGE
??????

k	G_k	σ_k [arcsec]
1	0.184	0.038
2	0.485	0.085
3	0.222	0.169
4	0.109	0.487

Table 3. F814W MGE???

k	total luminosity L_k [counts]	surface density $I_{0,k}$ [L_\odot/pc^2]	Gaussian dispersion		axis ratio
			σ_k [arcsec]	σ_k [kpc]	q'_k
1	9425.96	20768.	0.051	0.103	1.00
2	13173.0	3161.2	0.178	0.358	0.76
3	40235.0	1588.2	0.503	1.008	0.58
4	67755.2	502.25	1.180	2.368	0.56
5	203677.	136.51	3.891	7.805	0.57

4.2 Mass distribution from Lensing

Best fit lens model. The best fit lens model for the image positions in tab. 1 is given in the first column of tab. 5. Fig. 4a shows the corresponding critical curve, caustic and Einstein radius, and the best fit source position. In this case, where $\alpha = 1$, the critical curve is also an equidensity contour of the galaxy model. Fig. 4b overplots the smoothed residuals from the F814W image subtracted by the IRAF ellipse fit to the surface brightness with the contours of the best fit model's time delay surface. This demonstrates that, although we did not include any information about the shape of the lensing images in the fit, it is consistent with the predicted distortion for an extended source by the best fit lens model.

To estimate how the uncertainties in the determination of the image positions and galaxy center affect the results, we Monte Carlo sample random positions from a two-dimensional Normal distribution centered at the positions in tab. 1 and a standard deviation corresponding to the measurement error of 1 pixel. A Gaussian fit to the resulting distributions of best fit values leads to the constraints on the shape parameters and Einstein quantities in the second column in tab. 5. We therefore constrain the Einstein radius to within 2%, $R_{\text{ein}} = (0.91 \pm 0.02)$ arcsec and the projected mass within the critical curve with a relative error of 4%, $M_{\text{crit}} = (7.9 \pm 0.3) \cdot 10^{10} M_{\odot}$. Our measurement of R_{ein} is consistent with that from Brewer et al. (2012), $R_{\text{ein,SWELLS}} = (0.96 \pm 0.04)$ arcsec. The relative difference between our critical mass and that of Brewer et al. (2012), $M_{\text{crit,SWELLS}} = (8.86 \pm 0.61) \cdot 10^{10} M_{\odot}$, is 13%.

Comparison with Light Distribution. Fig. 5b shows the surface mass distribution as predicted by the best fit model in tab. 5. We introduce random noise according to the uncertainties in the Fourier shape parameters to create a mock observation that visualizes the effect of the measurement errors. To be able to compare the predicted mass distribution to the observed light distribution we transform the surface brightness into a mass density: We first integrate the MGE in tab. 3 to get the total luminosity within the Einstein radius and the predicted mass-to-light ratio as $\Upsilon_{\text{I,ein}} = M_{\text{ein}}/L_{\text{I,ein}}$. Fig. 5a shows then the observed surface brightness in the F814W filter multiplied by $\Upsilon_{\text{I,ein}}$. Fig. 5c finally compares equidensity contours at the same values of both the predicted lens mass distribution and the observed surface brightness times $\Upsilon_{\text{I,ein}}$. We note the following three facts: 1. The mass predicted from lensing and the observed light distribution are oriented in the same direction. 2. Within the Einstein radius mass and light distribution have the same shape, while further out the mass distribution is more roundish. 3. The light distribution drops faster than the mass with increasing radius. This could indicate that the stellar component of the galaxy is superimposed by a more roundish dark matter component.

[TO DO: Stuff to mention]

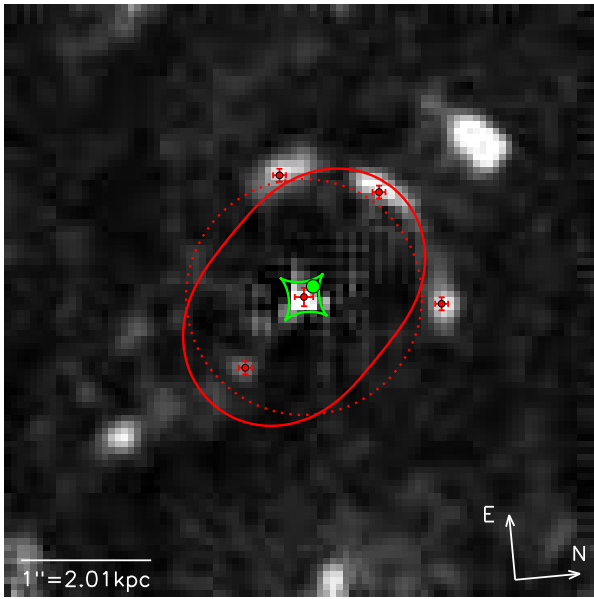
- best fit lens total mass distribution of J1331 has the same position angle and a similar elliptical shape as the surfache brightness distributon, but is slightly rounder, and could be consistent with a flat rotation curve.

Table 6. ???

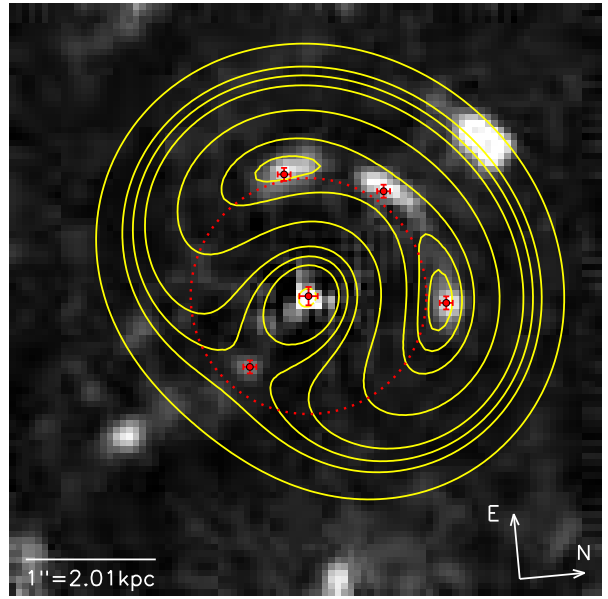
Total I-band luminosity within R_{ein} $L_{\text{I,ein}} [10^{10} L_{\odot}]$	Mass-to-light ratio within R_{ein} $\Upsilon_{\text{I,ein}} = M_{\text{ein}}/L_{\text{I,ein}} [\Upsilon_{\odot}]$
1.40	5.56

Table 5. ??? in tab. 1, for $\alpha = 1$

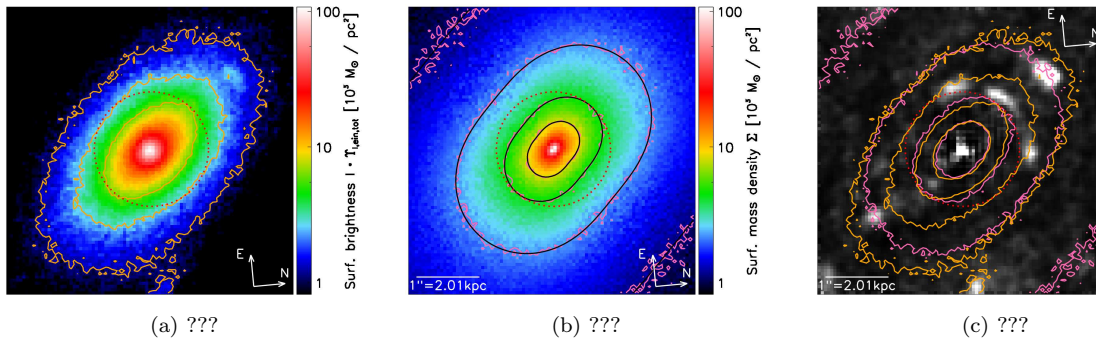
		lens model for peak image positions		lens model from Monte Carlo sampling of image positions		
Einstein Radius	R_{ein} [arcsec]	0.907	0.91	\pm 0.02	(2%)	
Einstein Mass	M_{ein} [$10^{10} M_{\odot}$]	7.72	7.8	\pm 0.3	(4%)	
Critical Mass	M_{crit} [$10^{10} M_{\odot}$]	7.87	7.9	\pm 0.3	(4%)	
Source Position	ξ [arcsec]	0.095	0.09	\pm 0.03	(28%)	
	η [arcsec]	0.107	0.10	\pm 0.03	(27%)	
Fourier Coefficients	a_0	1.814	1.82	\pm 0.04	(2%)	
	a_2	0.012	0.011	\pm 0.004	(35%)	
	b_2	-0.057	-0.06	\pm 0.01	(25%)	
	a_3	-0.0001	0.0000	\pm 0.0006		
	b_3	-0.0002	0.000	\pm 0.001		



(a) ??? Critical curves, Einstein radius, caustics, source position for best fit model. ??? [TO DO: nice caption]



(b) ??? Time delay surface ??? [TO DO: nice caption]

Figure 4. ???

(a) ???

(b) ???

(c) ???

Figure 5. ??? Preliminary crappy caption: Left: OBSERVED surface brightness multiplied by M/L in Einstein radius (overplotted in red). Middle: BEST FIT MODEL for mass distribution from lensing (including "wiggles" due to uncertainties in image positions). Contours are at the same levels. Right: Same contours, to directly show the difference in shape. ??? [TO DO: nice caption]

4.3 JAM based on Surface Brightness

... with "Mass-follows-Light" and Velocity Anisotropy

[TO DO]

... with Increasing Mass-to-Light Ratio Gradient

[TO DO]

... with the Lens Mass Model

[TO DO]

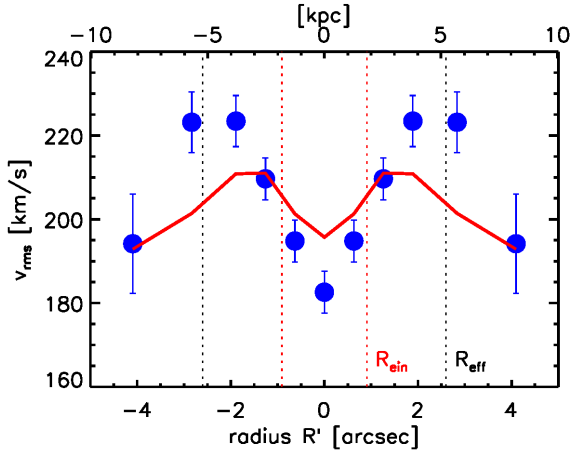


Figure 6. ??? Preliminary crappy caption: Failed try to fit a mass-follows-light model to the central regions of the galaxy. "Best fit" velocity anisotropy $\beta = -1/2$ is pegged at lower limit. ??? [TO DO: nice caption]

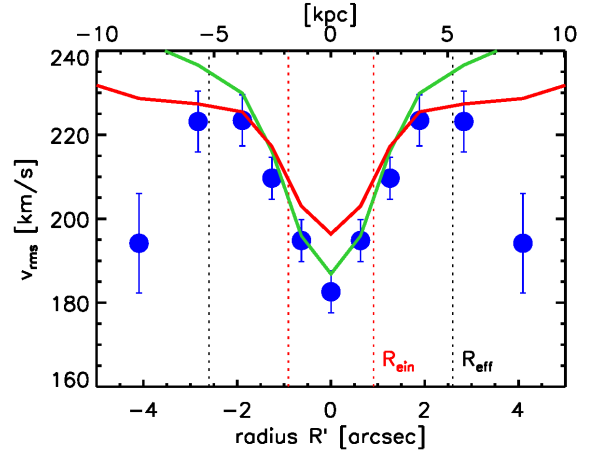
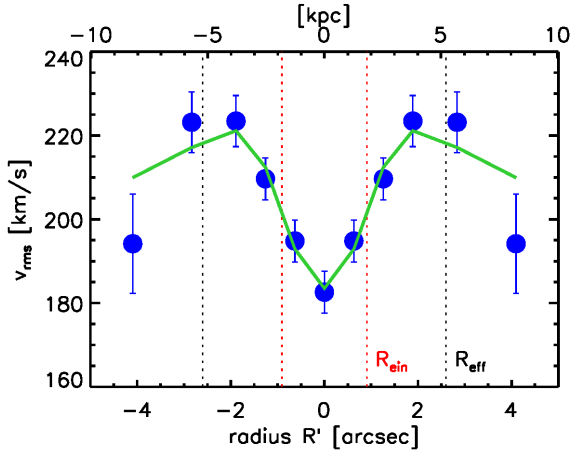
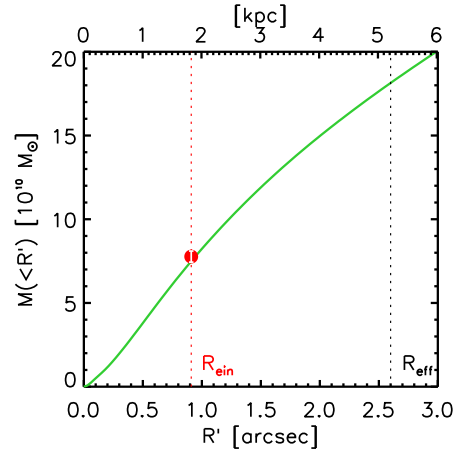


Figure 7. ??? Preliminary crappy caption: Observed v_{rms} is overplotted (not fitted) with best fit lens mass models for $\alpha = 1$ (red) and $\alpha = 1.1$ (green). ??? [TO DO: nice caption]



(a) ???



(b) ???

Figure 8. ??? Using the surface brightness MGE for the dynamical modelling: each Gaussian got it's own M/L such that the overall M/L is increasing with radius. This is the best fit model. The enclosed mass is overplotted with Einstein mass with 4% error (overplotted, not fitted). ??? [TO DO: nice caption]

4.4 JAM with a NFW Dark Matter Halo

Sampling with a Markov Monte Carlo Chain

[TO DO]

Predicting the Rotation Curve at larger Radii

[TO DO]

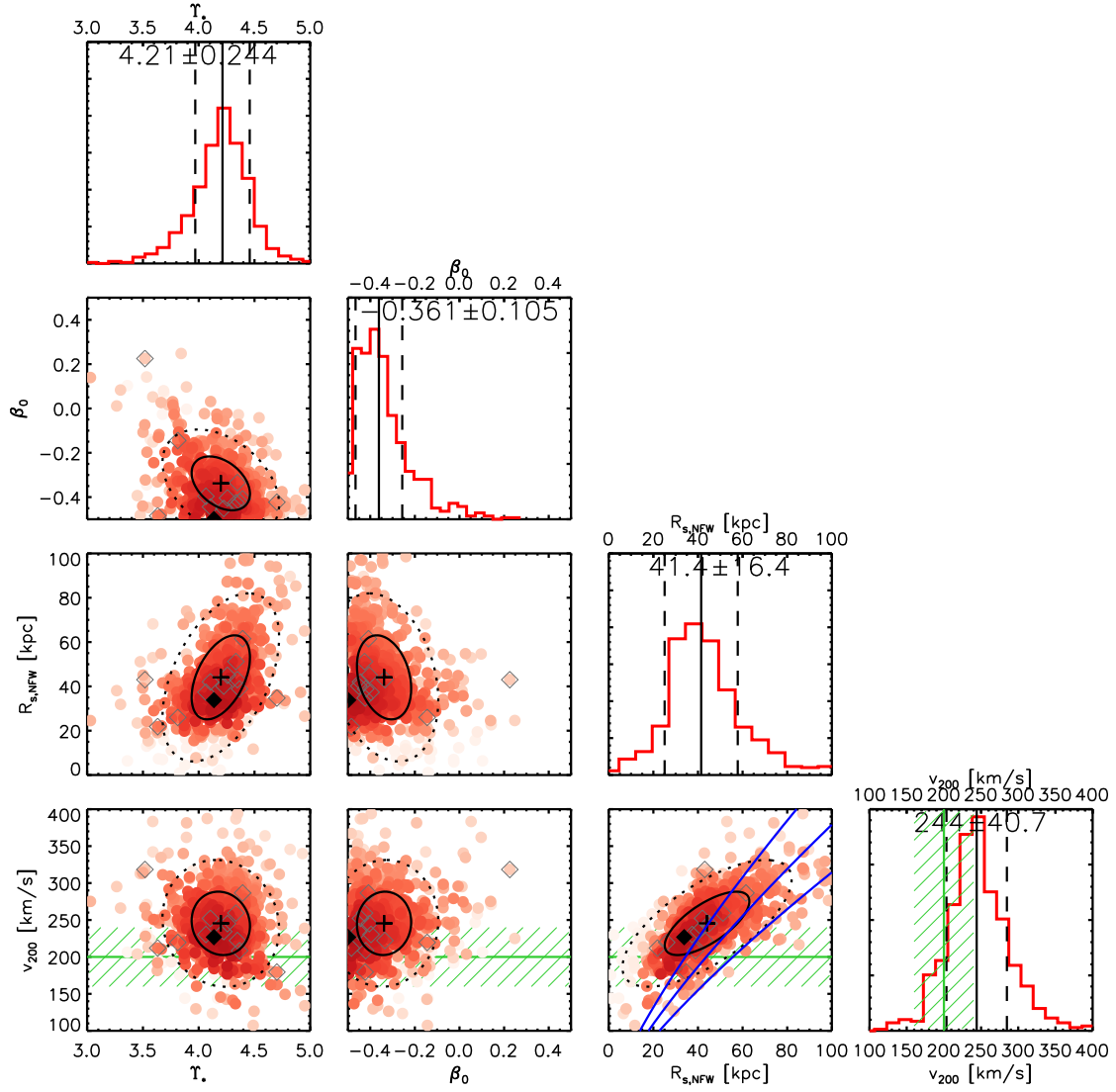


Figure 9. ??? Preliminary crappy caption: Result of the MCMC sampling of the parameter space for a model with NFW halo and constant velocity anisotropy. Green and blue shows the priors. Grey diamonds are the models shown in next figure. ??? [TO DO: nice caption]

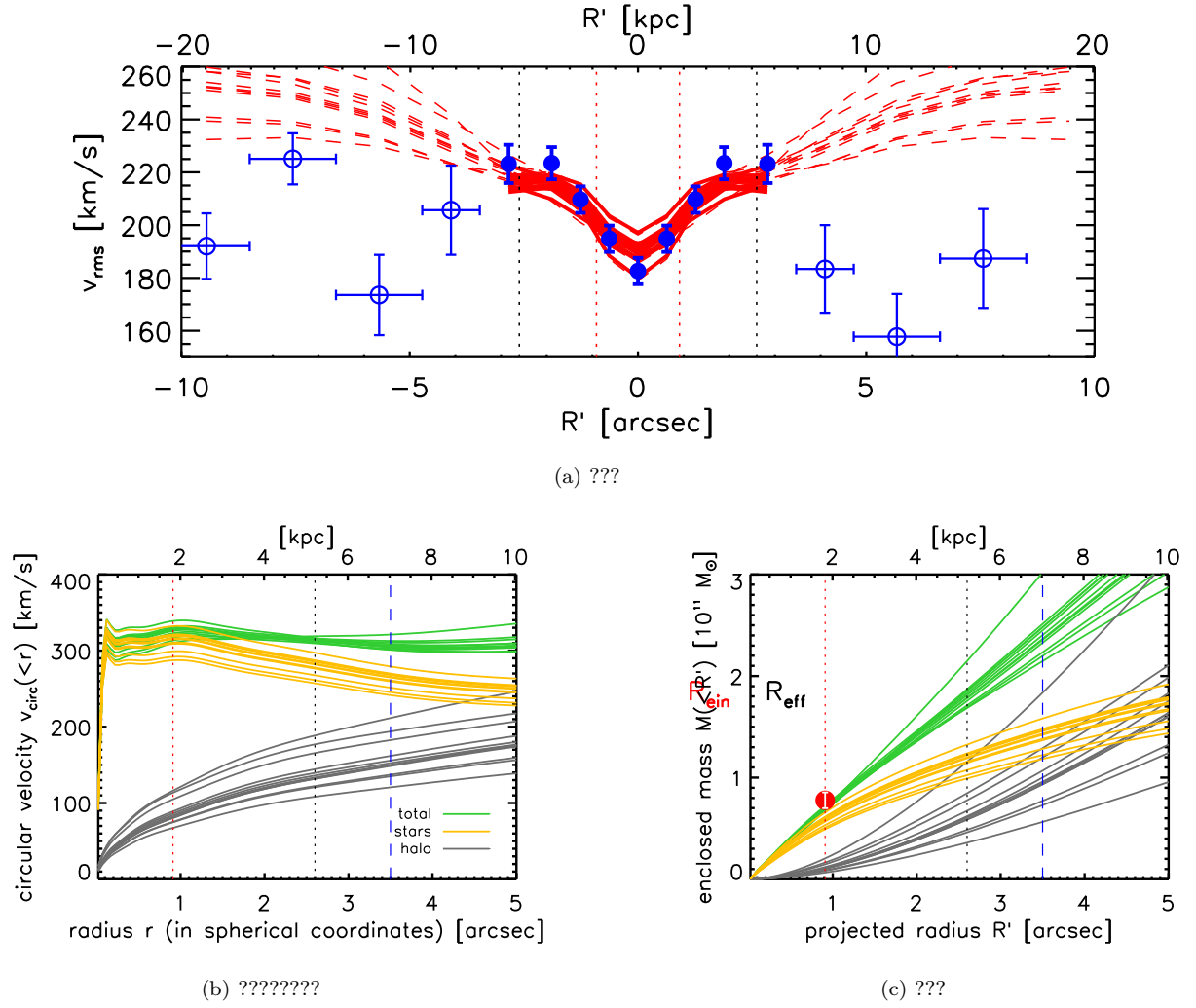


Figure 10. ??? Preliminary crappy caption: 12 samples from the parameter pdf found with the MCMC above for the model with NFW halo and constant velocity anisotropy. Big red dot shows the Einstein mass with a 10% error (used in fit). ??? [TO DO: nice caption]

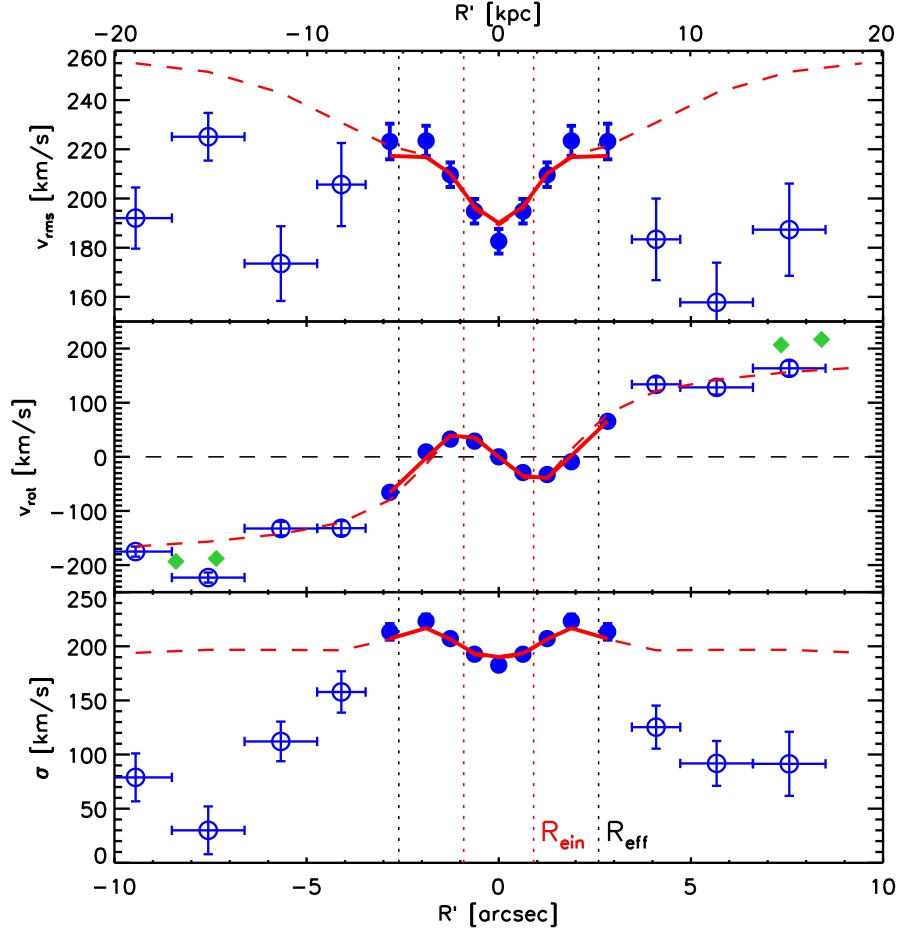


Figure 11. ??? Preliminary crappy caption: Model: NFW halo and constant velocity anisotropy, using the the mean / peak values of the MCMC result in the above pdf for the model parameters. Fitting one more free parameter to the rotation curve in the inner regions, predicting the rotation curve and dispersion at larger radii. Green dots are gas kinematics. ??? [TO DO: nice caption]

5 DISCUSSION AND CONCLUSION

5.1 Does J1331 have a Merger History?

[TO DO]

5.2 Summary

[TO DO]

REFERENCES

- Brewer B. J., Dutton A. A., Treu T., Auger M. W., Marshall P. J., Barnabè M., Bolton A. S., Koo D. C., Koopmans L. V. E., 2012, *Monthly Notices of the RAS*, 422, 3574
- Dutton A. A., Treu T., Brewer B. J., Marshall P. J., Auger M. W., Barnabè M., Koo D. C., Bolton A. S., Koopmans L. V. E., 2013, *Monthly Notices of the RAS*, 428, 3183
- Evans N. W., Witt H. J., 2003, *Monthly Notices of the RAS*, 345, 1351
- Kochanek C. S., 1991, *Astrophysical Journal*, 373, 354
- Narayan R., Bartelmann M., 1999, in Dekel A., Ostriker J., eds, *Formation of Structure in the Universe*, *Proceedings of the 1995 Jerusalem Winter School Lectures on Gravitational Lensing*. Cambridge University Press, pp 360–432
- Treu T., Dutton A. A., Auger M. W., Marshall P. J., Bolton A. S., Brewer B. J., Koo D. C., Koopmans L. V. E., 2011, *Monthly Notices of the RAS*, 417, 1601
- van de Ven G., Falcón-Barroso J., McDermid R. M., Cappellari M., Miller B. W., de Zeeuw P. T., 2010, *Astrophysical Journal*, 719, 1481